Pergamon

Materials Research Bulletin 36 (2001) 2485–2496

Materials Research Bulletin

Nuclear and magnetic structure of Ca_2MnWO_6: A neutron powder diffraction study

A.K. Azad[a,c,*], S.A. Ivanov[b], S.-G. Eriksson[a,c], J. Eriksen[a], H. Rundlöf[d], R. Mathieu[e], P. Svedlindh[e]

[a]*Studsvik Neutron Research Laboratory, Uppsala University, SE-611 82 Nyköping, Sweden*
[b]*Karpov Institute of Physical Chemistry, 103064 Moscow, Russia*
[c]*Department of Inorganic Chemistry, University of Gothenburg, SE-412 96 Göteborg, Sweden*
[d]*Department of Materials Chemistry, The Ångström laboratory, Box 538, SE-751 21 Uppsala, Sweden*
[e]*Department of Materials Science, Uppsala University, Box 534, SE-751 21 Uppsala, Sweden*

(Refereed)
Received 23 April 2001; accepted 11 June 2001

Abstract

The nuclear and magnetic structures of the double provskite compound Ca_2MnWO_6 have been determined by neutron powder diffraction. Rietveld refinement shows that the compound adopts a monoclinic crystal structure with $P2_1/n$ symmetry. Magnetic refinement at 10 K shows that the magnetic structure is based on a unit cell related to that of the nuclear structure by a propagation vector (0 1/2 1/2), which is not very common in the case of double perovskites. The crystal contains alternating MnO_6 and WO_6 octahedra, considerably tilted due to the relative small size of the cation that occupy the A-sublattice of the perovskite. The manganese magnetic moments are coupled antiferromagnetically along the unit cell axes with the magnetic moment equal to 3.49(2) μ_B (M_x = 1.08(13) μ_B, M_y = 0.94(7) μ_B, M_z = 3.20(4) μ_B). Antiferromagnetic behavior was confirmed by magnetization measurements, and the antiferromagnetic to paramagnetic transition was found at 16 ± 0.1 K.

Keywords: A. Magnetic materials; A. Oxides; C. Neutron scattering; D. Crystal structure; D. Magnetic structure

* Corresponding author.
E-mail address: azad@studsvik.uu.se (A.K. Azad).

0025-5408/01/$ – see front matter
PII: S0025-5408(01)00708-5

1. Introduction

Since half-metallic ferromagnetism and magnetoresistance (MR), especially at low temperature, seem to be intimately related to each other, there is an intensive search for half-metallic ferromagnets, which could be candidate materials for the realization of MR applications. While several double perovskite oxides of the kind $A_2B'B''O_6$ have been theoretically predicted to be half-metallic antiferromagnets [1], one such material, Sr_2FeMoO_6 [2] has recently [3,4] been shown to be a half-metallic ferromagnet, exhibiting a significant tunnelling type magnetoresistance at room temperature. Lattice anomalies associated with changes in spin alignment and/or electron transfer are often observed, which suggest a correlation between spin configuration and lattice. Static and/or dynamic Jahn-Teller distortions of the MnO_6 octahedra are also suspected to play an important role in the observed behavior [5]. The crystal system of double perovskites may adopt different distortions, because the B′(B″)-cation arrangement is limited to be of random type, rock salt type or of layered type.

The modification of structural and magnetic properties by changing the A, B′ and/or B″ site cations has gained interest in recent years to better understand the mechanism of colossal magnetoresistance (CMR) [6–8]. Depending on their valences and relative radii, transition metals often occupy the B-site, which can accommodate two different metal ions. It is now evident that the ferromagnetic transition temperature of mixed-valence manganites of the type $(R_{1-x}A_x)MnO_3$ cannot be increased above 400 K by any manipulation of the cation composition or the oxygen stoichiometry [9]. Considerably higher transition temperatures are needed for devices that rely on spin-polarized transport in half-metallic oxides if they are supposed to operate in a temperature range around room temperature. Depending on the ionic radius of the A-site cations, the crystallographic structure can adopt different structures [10]. For instance, when Ca^{2+} cations occupy the A positions in double perovskites, the structural symmetry lowers considerably. Ca_2FeMoO_6 and Ca_2FeReO_6 were found to be monoclinic [11,12] with ferromagnetic transition temperatures of 380 and 385 K, respectively. Ca_2FeWO_6 [13] was found to crystallize in the orthorhombic space group Pmm2, and showing a first-order structural phase transition at 706 ± 5°C.

We have already studied the related compounds Ba_2MnWO_6 [14] and Sr_2MnWO_6 [15]. Ba_2MnWO_6 is cubic [space group Fm-3m and $a = 8.1985(2)$], while Sr_2MnWO_6 crystallizes in the tetragonal space group $P4_2/n$ [$a = 8.0119(4)$, $c = 8.0141(8)$]. These results encouraged us to prepare and characterize a new compound Ca_2MnWO_6 (CMW). As a continuation of our research on double perovskites with unusual properties, we have synthesised single-phase material and performed X-ray and neutron diffraction studies to determine the nuclear and magnetic structures. Magnetic transition temperatures were found from low-field magnetization versus temperature measurements.

2. Experimental

Single-phase CMW powder was prepared by a standard solid-state reaction method. Stoichiometric amounts of the high purity reactants $CaCO_3$, MnO, and WO_3 were mixed and

sintered at temperatures up to 1340°C with several intermediate regrindings, followed by sintering at consecutively higher temperatures, always in a nitrogen environment. X-ray diffraction patterns were obtained from Guinier film data ($CuK_{\alpha 1}$ = 1.540598 Å). X-ray diffraction data were also collected on a Siemens D5000 diffractometer (CuK_{α} radiation) in the 2θ range from 15° to 60°. The data were collected with a 0.02° step size and a count time of 7 s/ step. Indexing and refinement of the lattice parameters were made with the programs TREOR90 [16] and PCPIRUM [17].

Neutron powder diffraction data were collected at the 50MW R2 Research Reactor at Studsvik, Sweden. The double monochromator system consisting of two parallel copper crystals in (220) mode was aligned to give a wavelength of 1.470(1) Å. The neutron flux at the sample position was approximately 10^6 neutrons $cm^{-2}s^{-1}$. Corrections for absorption effects were subsequently carried out in the Rietveld refinements, utilizing the empirical value $\mu R = 0.1168$ cm^{-1}. A vanadium can was used as the sample holder. The step scan covered a 2θ range 4–139.92°, with a step size of 0.08°. Diffraction data sets were refined by the Rietveld method using the FullProf software [18], with scattering lengths supplied by the software. Diffraction peakshapes were quantified by a pseudo-Voigt function, with a peak asymmetry correction applied at angles below 45° in 2θ. Background intensities were described by a Chebyshev polynomial with six coefficients. Each structural model was refined to convergence, with the best result selected on the basis of agreement factors and stability of the refinement.

Magnetization measurements were carried out using a QuantumDesign Superconducting QUantum Interference Device (SQUID) magnetometer. Magnetization versus temperature curves were measured between 5 to 200 K in field-cooled (FC) and zero field-cooled (ZFC) modes with applied fields ($\mu_0 H$) up to 1T. Environmental Scanning Electron Microscopy (ESEM) and Energy Dispersive X-ray (EDX) measurements were performed in a Philips XL30 ESEM at an acceleration voltage of 20 kV. The energy dispersive analyses confirm that the actual cationic composition of the perovskite-related crystallites was close to the nominal one, and was homogeneous all over the sample.

3. Results and discussion

3.1. Refinement of the crystal structure at 295 K

Rietveld structure refinements of the NPD data confirm the single-phase nature of the sample with cationic and anionic stoichiometry close to the idealized formula of Ca_2MnWO_6 (Fig. 1 and Table 1). CMW is distorted, showing monoclinic symmetry (space group $P2_1/n$) with a = 5.4617(1) Å, b = 5.6545(1) Å, c = 7.8022(3) Å and β = 90.193(3)°. Unit cell parameters are related to the ideal cubic perovskite as $a \approx \sqrt{2}a_0$, $b \approx \sqrt{2}a_0$, and $c \approx 2a_0$ ($a_0 \approx 3.8$ Å). Twelve positional parameters, 6 isotropic thermal parameters, 476 reflections, and a total of 36 refined parameters converged with R_p = 3.01%, R_{wp} = 3.85%, R_{Bragg} = 1.81% and χ^2 = 2.34. Fig. 2 shows the polyhedral view of CMW, where the ($a^-b^-b^-$) tilting (Glazer's notation) [19] of MnO_6 and WO_6 octahedra is readily apparent together with the distribution of Mn and W ions over the B sites.

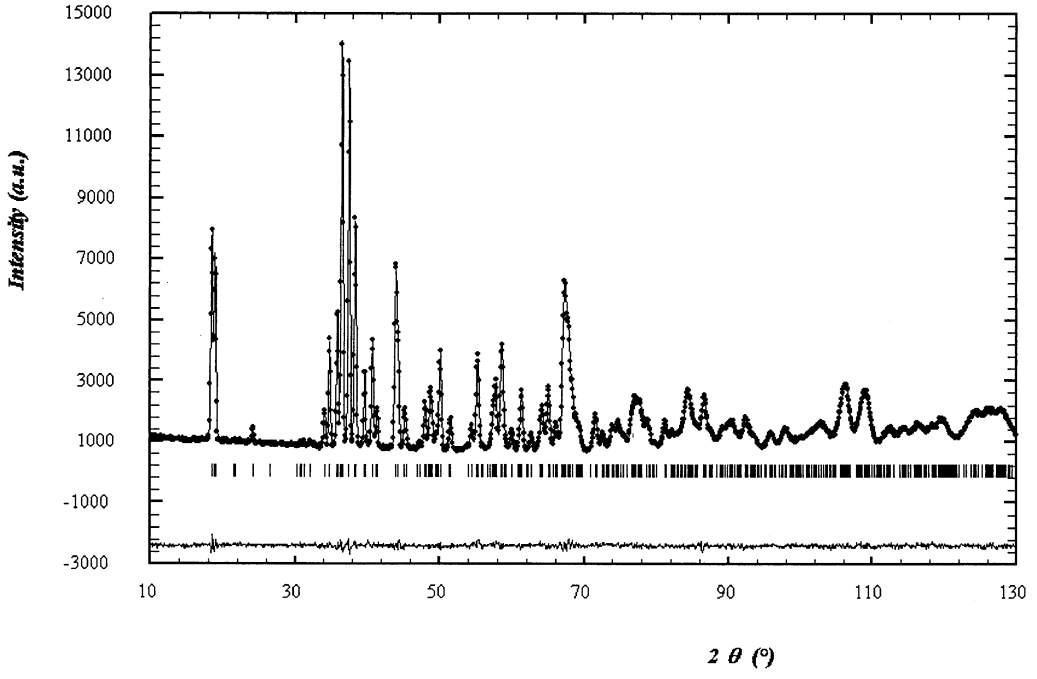

Fig. 1. Observed (circles) and calculated (continuous line) NPD intensity profiles for Ca_2MnWO_6 at room temperature (295 K). The short vertical lines indicate the angular position of the allowed Bragg reflections. At the bottom in each figure the difference plot, $I_{obs} - I_{calc}$, is shown.

3.2. Determination and refinement of the magnetic structure at 10 K

The 10 K NPD data (cf. Fig. 3) reveal a number of pure magnetic reflections at low 2θ-angles (2θ = 9.17, 17.99, 23.12, 23.74, 27.94, 32.03, 32.66, and 42.49°). These additional reflections could be indexed according to a magnetic unit cell with lattice parameters $a_m = a_n$, $b_m = 2b_n$, and $c_m = 2c_n$, where m and n refer the magnetic and nuclear unit cells, respectively. For analysis of the low-temperature NPD data a multi-pattern refinement was performed. The magnetic structure was refined in space group P1 as an independent phase for which only the Mn^{2+} cations were defined and only magnetic scattering was calculated. The different structures were modelled with magnetic moments at the Mn positions. The model was refined with reflections in the 2θ-range 4–62°. The final result of the refinement is shown in Fig. 4. After the full refinement of the profile, including the magnitude of the magnetic moment and its orientation, a best discrepancy factor R_{mag} of 4.83% was reached for an antiferromagnetic (AF) model (see Fig. 5). Table 1 includes the unit cell, atomic, and thermal parameters and the discrepancy factors at 295 and 10 K. The three components of the magnetic moment, $M_x = 1.08(13)\ \mu_B$, $M_y = 0.94(7)\ \mu_B$ and $M_z = 3.20(4)\ \mu_B$, yielded a total magnetic moment of $3.49(2)\ \mu_B$. Fig. 5 shows the orientation of the magnetic moments in the unit cell.

Table 1
Main crystallographic and magnetic information for Ca_2MnWO_6 (s.g. $P2_1/n$, Z = 2) from NPD Data at different temperatures

	295 K	10 K	
	Nuclear phase	Nuclear phase	Magnetic phase
a (Å)	5.4618 (2)	5.4457 (2)	5.4457 (2)
b (Å)	5.6545 (2)	5.6529 (2)	11.3058 (3)
c (Å)	7.8022 (3)	7.7828 (3)	15.5656 (6)
β (deg)	90.192 (3)	90.229 (4)	90.229 (4)
V (Å^3)	240.96 (1)	239.58 (2)	958.3427 (8)
	Ca in 4*e*(*x y z*)		
x	0.0142 (6)	0.0136 (5)	
y	−0.0533 (4)	−0.0551 (4)	
z	0.2494 (4)	0.2477 (4)	
B (Å^2)	0.82 (5)	0.29 (4)	
	Mn in 2*d*(*0 ½ 0*)		
B (Å^2)	0.36 (8)	0.014 (69)	
Magnetic moment (μ_B)			3.49 (2)
	W in 2*b*(*½ 0 0*)		
B (Å^2)	0.12 (6)	0.053 (56)	
	O1 in 4*e*(*x y z*)		
x	0.2152 (4)	0.2143 (4)	
y	0.1857 (4)	0.1866 (4)	
z	0.0459 (3)	0.0465 (3)	
B (Å^2)	0.53 (5)	0.25 (5)	
	O2 in 4*e*(*x y z*)		
x	0.1812 (4)	0.1813 (3)	
y	0.2187 (4)	0.2178 (4)	
z	0.4459 (3)	0.4432 (3)	
B(Å)	0.53 (5)	0.21 (3)	
	O3 in 4*e*(*x y z*)		
x	0.5962 (4)	0.5985 (4)	
y	0.0357 (3)	0.0373 (3)	
z	0.2350 (3)	0.2347 (3)	
B (Å^2)	0.47 (5)	0.29 (4)	
	Reliability factors		
R_p(%)	3.01	2.67	
R_{wp}(%)	3.85	3.55	
R_B(%)	1.81	1.70	
χ^2	2.34	1.87	
R_{mag}(%)			4.83

3.3. Discussion about the crystal and magnetic structures

In the $P2_1/n$ space group, it is necessary to define two crystallographically independent B positions (for Mn and W), as well as three kinds of nonequivalent oxygen positions (O1, O2, and O3), all in general (*x, y, z*) positions. The monoclinic β angle is only slightly different from 90°, ~90.192°, the metric of this structure seems to be strongly pseudo-orthorhombic. The three inequivalent oxygen positions can be precisely determined by NPD because neutrons are more sensitive to the oxygen positions than X-rays are. The 2*d* and 2*b* sites were fully occupied by Mn and W atoms, respectively. No mixing of sites between Mn and W was

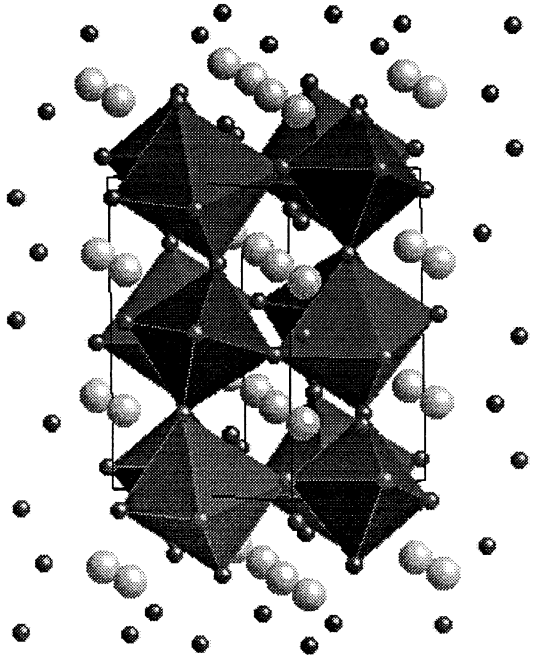

Fig. 2. The crystal structure of the monoclinic perovskite Ca_2MnWO_6; larger spheres represent the A-site cations and smaller spheres represent the oxygen.

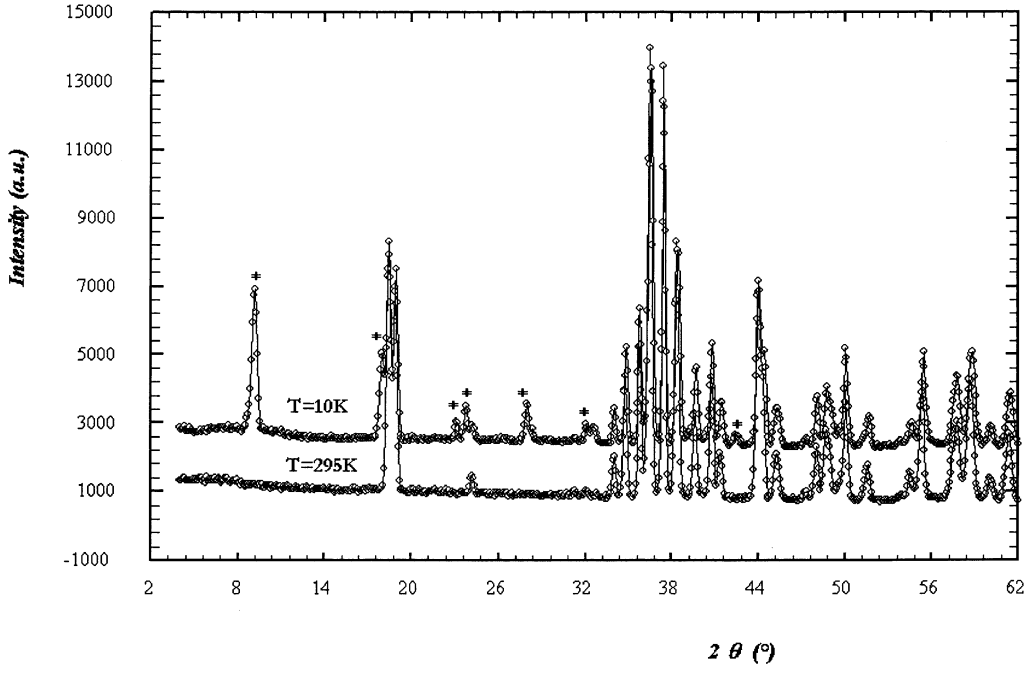

Fig. 3. Observed diffraction patterns at T = 295 K and 10 K in the 2θ range 10–60°. The extra reflections of magnetic origin are indicated by ‡.

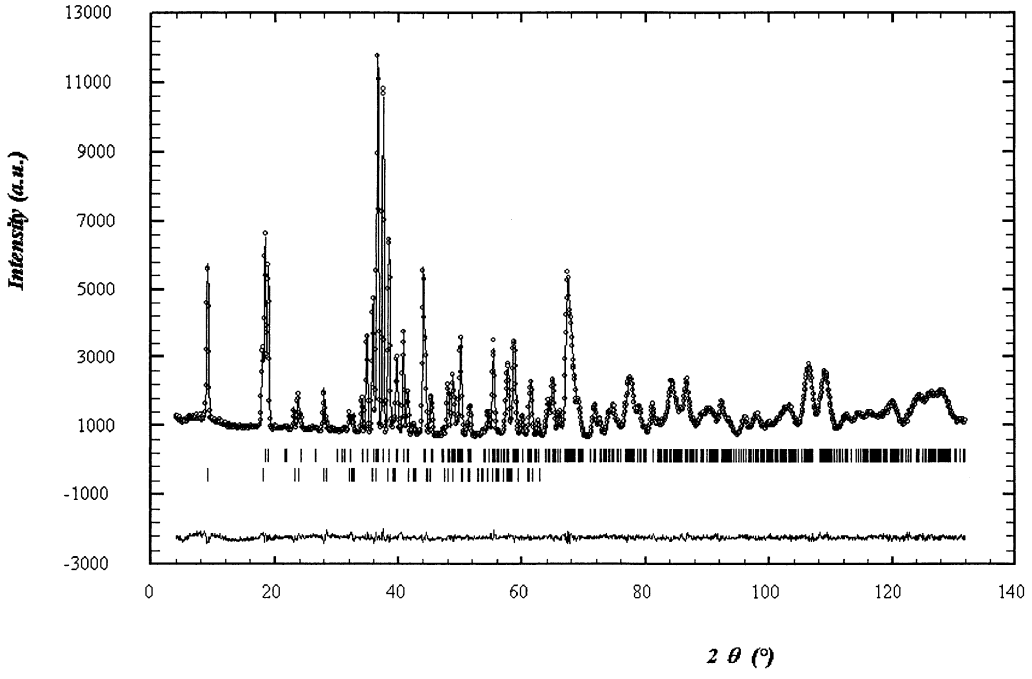

Fig. 4. Observed (dots), calculated (lines), and difference (bottom) plots of NPD Rietveld profiles at 10 K.

found during the refinement. The crystal structure of CMW is considerably distorted due to the small size of Ca^{2+} cations (tolerance factor, t = 0.916), which force the $(Mn,W)O_6$ octahedra to tilt to optimize the Ca–O bond distances. The MnO_6 and WO_6 octahedra are fully ordered and alternate along the three directions in the crystal structure in such a way that each MnO_6 octahedra is linked to six WO_6 octahedra, and vice versa (see Fig. 2). Several examples of monoclinically distorted perovskites have been described in the introduction [10–12]. In all these cases the compound crytallizes in space group $P2_1/n$ and show long-range ordering between the two different cations placed in the B′ and B″ positions. The driving force for the B′ and B″ ordering is the size and charge difference between both kinds of cations, for instance Fe^{3+} and Mo^{5+} in Ca_2FeMoO_6. It is remarkable that all of these compounds show an extraordinarily high pseudo-orthorhombic character as far as unit cell dimensions are concerned: β angles are very close to 90°, for example, β = 89.969(8)° for Ca_2FeMoO_6 [12] and 90.4° for Ca_2FeReO_6 [13].

Because the sixfold-coordinated ionic radii for Mn^{2+} and W^{6+} ions are 0.97 Å and 0.74 Å, respectively [20], there will be a tendency for Mn^{2+} ions to occupy larger octahedral sites than W^{6+} ions. The MnO_6 octahedra (volume = 13.4105(2) $Å^3$) is significantly larger than the WO_6 octahedra (volume = 9.4870(9) $Å^3$). Due to the $P2_1/n$ symmetry, there is flexibility in the volumes of the individual BO_6 octahedra, thereby permitting a variety of different cation ordering patterns over the B-sites. The average B–O bond lengths at 295 K compare well with the expected values as calculated from ionic radii sums: [20] <Mn–O>, 2.1599(6) Å (calc 2.23 Å); <W–O>, 1.9164(1) Å (calc 2.00 Å). Calculation of bond valence sums

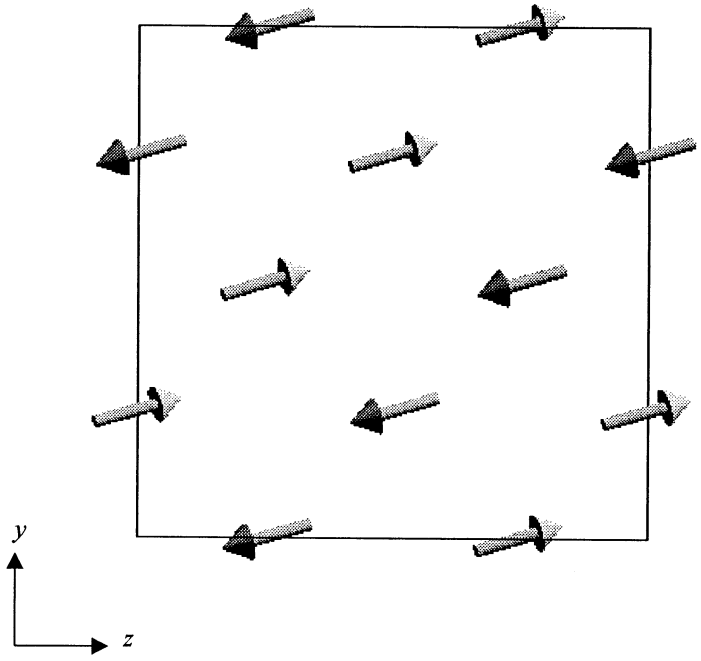

Fig. 5. The orientation of magnetic moments in Ca_2MnWO_6. The arrows indicate the direction of the magnetic moments at the Mn-sites (view x = 0).

(BVS), using the Brown's bond valence model [21], from the structural parameters, indicated that Mn and W cations seem to be in their divalent and hexavalent oxidation states, respectively. Average bond distances of <Mn–O> (2.1564(3) Å) and <W–O> (1.9191(3) Å) do not vary significantly at 10 K, indicative of the relative stability of the structure. Main bond distances and bond angles are listed in Table 2. A strong tilting of the BO_6-octahedra compared with the ideal cubic structure can be realized by looking at the Mn–O–W bond angles.

The *z*-component of the moment contributes most strongly to the total magnetic moment. The extra magnetic peaks, which appear at 10 K, have been indexed using the magnetic unit cell parametes $a = 5.4457(2)$ Å, $b = 11.3058(3)$ Å, and $c = 15.5656(6)$ Å, which was related to the chemical unit cell by the propagation vector $\mathbf{k} = (0\ 1/2\ 1/2)$. The unit cell dimension as well as the arrangement of magnetic moments are quite uncommon for antiferromagnetic double perovskites. For example, in Ba_2CoWO_6 and Ba_2NiWO_6 [22] the magnetic unit cell is doubled along all three unit-cell axes. The magnetic structure in Ca_2MnWO_6 can be described as alternating set of (011) ferromagnetic planes coupled antiferromagnetically (+ − + −) (see Fig. 5).

3.4. Magnetization measurements

Fig. 6 shows the FC (M_{FC}/H) and ZFC (M_{ZFC}/H) magnetization versus temperature curves for Ca_2MnWO_6. They were measured with the applied fields $\mu_0 H = 0.002$ T, 0.05 T,

Table 2
Main bond distances (Å) ($d \leq 3.5$Å) and selected angles (deg.) for monoclinic Ca_2MnWO_6 determined from NPD data at 295 K and 10 K

	295 K	10 K
	MnO_6 Octahedra	
Mn–O1 (Å) (×2)	2.159 (8)	2.151 (6)
Mn–O2 (Å) (×2)	2.175 (8)	2.172 (2)
Mn–O3 (Å) (×2)	2.144 (3)	2.145 (5)
<Mn–O> (Å)	2.1599 (6)	2.1564 (3)
distortion (Δ)	0.01458	0.01238
	WO_6 Octahedra	
W–O1 (Å) (×2)	1.911 (7)	1.915 (2)
W–O2 (Å) (×2)	1.921 (2)	1.928 (2)
W–O3 (Å) (×2)	1.916 (3)	1.913 (7)
<W–O>(Å)	1.9164 (1)	1.9190 (3)
distortion (Δ)	0.00496	0.00756
Mn–O1–W (°) (×2)	149.719 (2)	149.561 (1)
Mn–O2–W (°) (×2)	147.182 (3)	146.265 (9)
Mn–O3–W (°) (×2)	147.715 (9)	146.882 (9)
	CaO_9 Polyhedra	
Ca–O1 (Å)	2.359 (1)	2.350 (4)
Ca–O1 (Å)	2.625 (7)	2.621 (6)
Ca–O1 (Å)	2.724 (2)	2.704 (3)
Ca–O2 (Å)	2.353 (3)	2.349 (1)
Ca–O2 (Å)	2.602 (1)	2.575 (2)
Ca–O2 (Å)	2.771 (3)	2.790 (1)
Ca–O3 (Å)	2.340 (3)	2.322 (1)
Ca–O3 (Å)	2.403 (9)	2.387 (8)
Ca–O3 (Å)	3.220 (5)	3.229 (4)

0.2 T, and 1 T, and the curve corresponding to the smallest field shows that a magnetic transition occurs at $T_c \sim 45$ K. The magnetic interactions are predominantly antiferromagnetic (AF), but below 45 K a small spontaneous moment develops, like in a canted-AF state [23], resulting in a magnetic state that can be described as a weak ferromagnetic state. The cusp around 20−40 K in the ZFC curves is another property that is found in the case of canted-antiferromagnetism [23]. The presence of a spontaneous moment is further emphasized by the magnetic irreversibility exhibited by the FC and ZFC curves; below the transition temperature, the ZFC and FC curves show large deviations. With increasing field, the transition is masked by the larger and linear in field AF-like response of the material. Magnetic hysteresis curves were measured at 10 and 40 K, confirming the existence of a weak ferromagnetic response but that the predominant character of the response is linear in field. This behavior is analogous to that observed for Ba_2MnWO_6 [14], where a canted-AF phase was observed below ~45 K. In the NPD data for Ba_2MnWO_6, diffuse magnetic scattering was observed in the temperature range from 10 to 50 K, which was explained by the existence of small magnetic domains, showing antiferromagnetic order, but being of a size too small to give rise to distinct magnetic Bragg peaks. Because for Ca_2MnWO_6 we do not observe distinct Bragg peaks at 40 K, it is our strong belief that also in this compound the canted-AF phase consists of small AF domains.

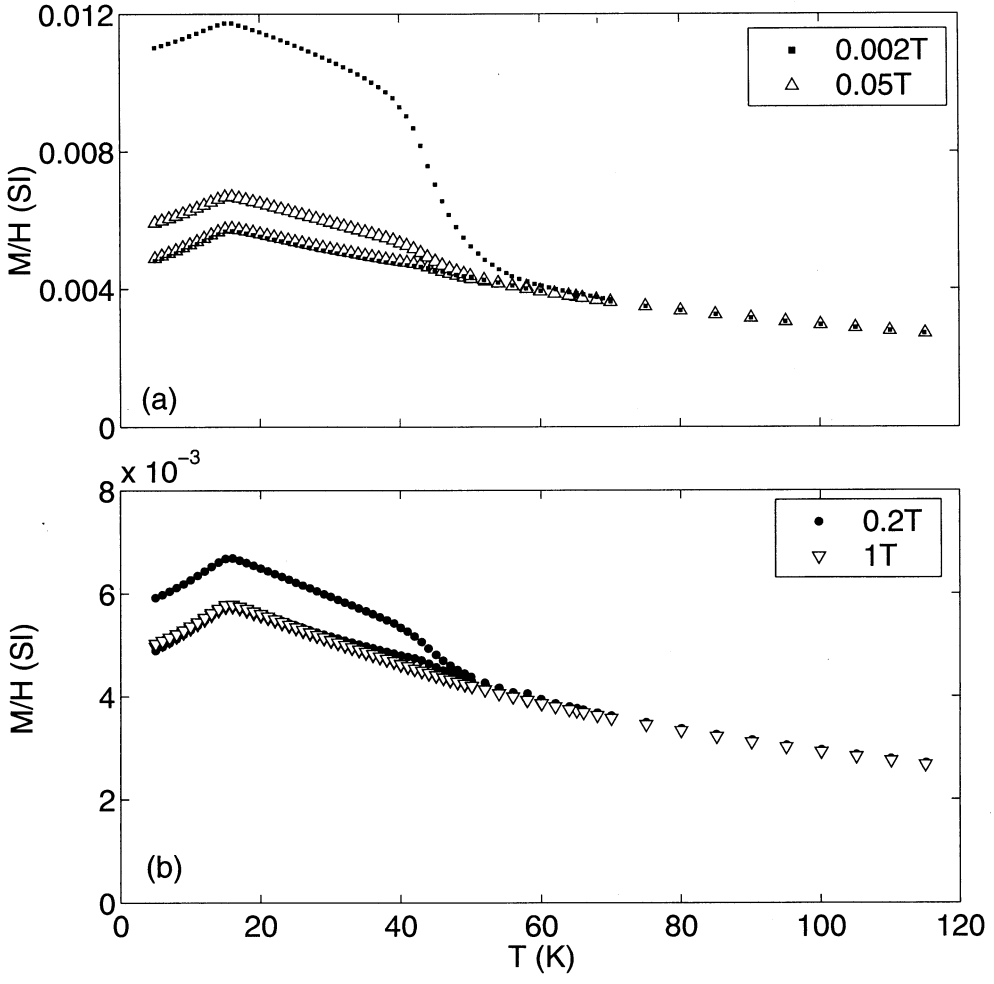

Fig. 6. M_{FC}/H and M_{ZFC}/H versus temperature for Ca_2MnWO_6 measured with the applied fields $\mu_0 H$ (a) 0.002 T and 0.05 T, and (b) 0.2 T and 1T.

On further lowering of the temperature, a transition to a low temperature AF phase is observed at $T_N = 16 \pm 0.1$ K, as also evidenced by the appearance of resolution limited magnetic Bragg peaks in the NPD data at 10 K. However, the magnetic state below T_N is not that of an ideal antiferromagnet, because magnetic irreversibility remains down to the lowest temperature studied. Thus, a small canting angle even exists below T_N giving rise to a net spontaneous magnetic moment.

Above the transition temperature T_c the sample shows typical Curie-Weiss behavior. The data were fitted to a Curie-Weiss law, $\chi = C/(T - \theta)$, where C is the Curie constant and θ is the Weiss temperature, yielding $C = 0.482$ and $\theta = -61.8$ K. The effective number of Bohr magnetons (p) is from these results calculated to be $p = 4.72$. The negative sign of the Weiss temperature indicates that the magnetic interaction between Mn ions is antiferromagnetic.

4. Conclusions

From X-ray diffraction data the single-phase nature of Ca_2MnWO_6 (CMW) was confirmed. Rietveld analysis of NPD data shows that this B-site ordered double-perovskite type oxide adopts a monoclinic structure, crystallizing in space group $P2_1/n$. The nuclear (or chemical) cell is related to the ideal cubic perovskite unit as $a \approx \sqrt{2}a_0$, $b \approx \sqrt{2}a_0$, and $c \approx 2a_0$ ($a_0 \approx 3.8$ Å). From BVS calculations the charge distribution between Mn and W ions in Ca_2MnWO_6 was obtained as Mn^{2+} and W^{6+}. The ZFC and FC magnetization measurements indicate a transition from a paramagnetic state to a weak ferromagnetic state at ~45 K. Furthermore, on lowering the temperature there is a transition to an AF state at 16 ± 0.1 K. Analysis of the 10 K NPD data supports the occurrence of an AF state at low temperature. The magnetic unit cell is related to the nuclear one as $a_m = a_n$, $b_m = 2 \times b_n$ and $c_m = 2 \times c_n$.

Acknowledgments

The authors are grateful to the Royal Swedish Academy, the Swedish Natural Science Research Council (NFR) and the Swedish Foundation of Strategic Research (SSF) for financial support. One of the authors, A.K. Azad, gratefully acknowledges the financial support from the "Research, development and training project of Bangladesh Atomic Energy Commission."

References

[1] W.E. Pickett, Phys. Rev. B 57 (1998) 10613.
[2] K.-I. Kobayashi, T. Kimura, H. Sawada, K. Terakura, Y. Tokura, Nature 395 (1998) 677.
[3] R.P Borges, R.M. Thomas, C. Cullinan, J.M.D. Coey, R. Suryanarayanan, L. Ben-Dor, L.P. Gaudart, A. Revcolevski, J. Phys. Condens. Matter 11 (1999) 445.
[4] B. Garcia-Landa, C. Ritter, M.R. Ibarra, J. Blasco, P.A. Algarabel, R. Mehendiran, J. Garcia, Solid State Commun.110 (1999) 435.
[5] A.J. Millis, B.I. Shraiman, R. Mueller, Phys. Rev. Lett. 77 (1996) 175.
[6] D. Iwanaga, Y. Inaguma, M. Itoh, J. Solid State Chem. 147 (1999) 291.
[7] A. Maignan, B. Raveau, C. Martin, M. Hervieu, J. Solid State Chem. 144 (1999) 224.
[8] K. Henmi, Y. Hinatsu, N.M. Masaki, J. Solid State Chem. 148 (1999) 353.
[9] J.M.D. Coey, M. von Molnárand, Viret. Adv. Phys. 48 (1999) 167.
[10] C. Ritter, M.R. Ibara, L. Morellon, J. Blasco, J. Garcia, J.M. De Teresa et al., Conds. Matter 12 (2000) 8295.
[11] J.A. Alonso, M.T. Casais, M.J. Martinez-Lope, J.L. Martinez, P. Velasco, A. Munoz et al., Chem. Mater 12 (2000) 161.
[12] W. Prellier, V. Smolyaninova, A. Biswas, C. Galley, R.L. Greene, K. Ramesha et al., Condens. Matter 12 (2000) 965.
[13] Fu-Zhengmin, Li-Wenxiu, Sci. China Series-A 38 (1995) 974.
[14] A.K. Azad, S. Ivanov, S.-G. Eriksson, J. Eriksen, H. Rundlöf, R. Mathieu et al., Mater. Res. Bull., Vol. 36, Issue 13, in press.
[15] A.K. Azad, S.-G. Eriksson, S. Ivanov, J. Eriksen, H. Rundlöf, R. Mathieu et al., Abstract of 17th Nordic Structural Chem. Meeting, Arhus, Denmark, 2001, p. 2.

[16] P.-E. Werner, Z. Kristallogr. 120 (1964) 375.
[17] P.-E. Werner, Ark. Kemi 31 (1969) 513.
[18] J. Rodrigues-Carvajal, Physics B 192 (1993) 55.
[19] A.M. Glazer, Acta Crystallogr. B28 (1972) 3384.
[20] R.D. Shannon, Acta Crystallogr. A 32 (1976) 751.
[21] I.D. Brown, in: M. O'Keefe, A. Navrotsky (Eds.), Structure and Bonding in Crystals, Academic Press, New York, vol. 2, 1981, pp.1–30.
[22] A. Oles, F. Kajzar, M. Kucab, W. Sikora, Magnetic Structures Determined by Neutron Diffraction, Panstwowe Wydawnictwo Naukowe, Poland, 1976.
[23] G. Amow, J.E. Greedan, C. Ritter, J. Solid State Chem. 141 (1998) 262.